Δελτίο Ελληνικής Γεωλογικής Εταιρίας τομ. XXXV, 108 - 117, 2003
Bulletin of the Geological Society of Greece vol. XXXV, 108 - 117, 2003

Thermal Imaging of Nisyros Volcano (Aegean Sea) using ASTER data

ATHANASIOS GANAS[1*], SPYRIDOULA VASSILOPOULOU[2], EVANGELOS LAGIOS[2] and VASSILIOS SAKKAS[2]

ABSTRACT

Three ASTER Level 1B scenes of the Nisyros Volcano (Aegean Sea, Greece) were processed for land surface temperature extraction. The scenes were acquired on April 26, 2002 (Day-time), June 13, 2002 (night-time), and October 26, 2002 (night-time). Band 13 (10.25-10.95 mm; 90 m spatial resolution) was processed using scene-specific standard atmospheres from the ATCOR atmospheric libraries that matched surface meteorological data collected at Rhodes and Kos islands for the first two scenes, and Nisyros during the third scene acquisition. The results show a good comparison with previously processed LANOSAT7 ETM+ thermal data during October 2000. The crater region was clearly located and it was mapped warmer than the surroundings within the range of temperatures measured over previous campaigns (22-24°C). The 2002 images show a temperature increase of 2 °C inside the Stefanos crater relative to previous work, which indicates thermal instability of this region over this two-year period.

1. Introduction

1.1 The Nisyros Setting

The Nisyros Volcano in the Aegean Sea has recently gained attention from the geosciences community because of its renewed activity during 1995-1997 (Figure 1; Papadopoulos et al., 1998; Lagios, 2000). Nisyros is a Quaternary strato-volcano of mainly andesitic-rhyolitic composition and about 7 km diameter in size. It is situated in the middle of an E-W graben between the Dodecanese islands of Kos and Tilos (Papanikolaou & Nomikou, 2001). The volcano mainly presents a 'hydrothermal' hazard (Marini et al., 1993). Today, it shows slow chemical changes of its fumaroles, which is accompanied by micro-earthquake activity and ground deformations (Lagios et al., 2001; Chiodini et al., 2002; Sachpazi et al., 2002).

1.2 The ASTER Sensor

ASTER is the acronym for Advanced Spaceborne Thermal Emission and Reflection Radiometer. It is a Japanese multispectral sensor carried on the TERRA satellite, which was launched on December 18, 1999. TERRA orbits the Earth with a period of 98.1 minutes at a height of 720 km. Data formats and applications are discussed in Abrams et al. (2001). ASTER is a narrow-field of view sensor (the swath angle of the sensor is ±2.4°), which scans a swath of 60 km on the ground every 16 days. The sensor has nine (9) reflective bands and five (5) bands in the thermal infrared (TIR), providing thus a wealth of spectral information to map geological surfaces. In the TIR region, ASTER has 12 bit quantization, a radiometric precision (NEΔT) of 0.3 °K, and one standard deviation calibration uncertainty of 1 °K between 270 and 340 °K.

[1] *Geodynamics Institute, National Observatory of Athens, P.O. Box 20048, Athens 118 10, Greece. *corresponding author. aganas@gein.noa.gr*

[2] *Space Applications Unit in Geosciences, Geophysics Laboratory, Dept. of Geophysics & Geothermics, University of Athens, Panepistimiopolis – Ilissia, Athens 157 84, Greece*

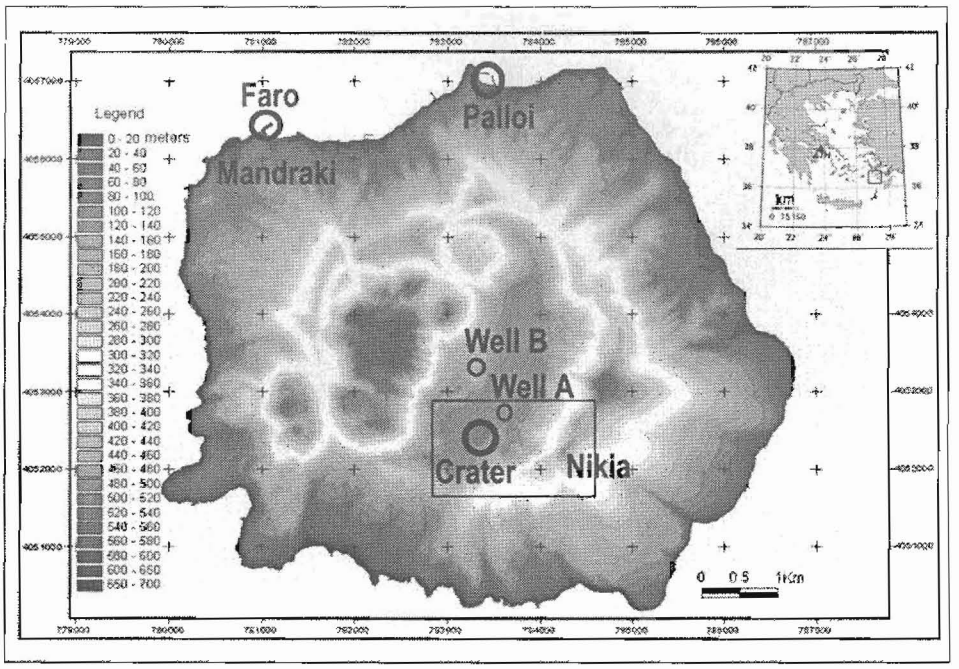

Figure 1. Elevation map of Nisyros Island showing ground data localities (black circles) during the October 2002 campaign. Inset box shows extent of Figure 2. Coordinate system is Greek 1987 (Transverse Mercator). Inset at upper right corner shows location of the area within Greece.

1.3 The ATCOR software

The Atmospheric Correction (ATCOR) program developed by DLR (Richter, 1996) and distributed by GEOSYSTEMS Gmbh (Geosystems, 2002) was used to process the ASTER data. The surface temperature image is calculated from the radiance registered at thermal band 13 (10.25-10.95 mm) of ASTER. Band 13 is the less affected by both water vapor and ozone absorptions (Thome et al., 1998). The software assumes that radiance is related to the grey value recorded at the sensor with a linear function, while its relationship to the brightness temperature (equivalent blackbody temperature) is given by Plank's law. The atmospheric transmission and path radiance are both estimated by the use of proper atmospheric models. In this work the atmospheric correction was done using a reference model from the software's atmospheric library, assuming a uniform surface emissivity of 0.98. The constant emissivity assumption was found to hold for most surfaces of the LANDSAT7 ETM+ night scene of Nisyros during October 2000 overpass (Ganas and Lagios, 2003). However, the bare surfaces of the Stefanos and Polivotis craters (Figure 2), where lithology is mainly composed by rhyolitic lavas, are expected to have an emissivity ranging between 0.94 – 0.96 (e.g. Kahle, 1987; Harris & Stevenson, 1997). The craters are located within an area of increased surface temperatures, because of the existence of low-temperature fumaroles (Brombach et al., 2001).

1. 4 Raw Data Characteristics

The ASTER level 1B scenes of Nisyros are registered radiance at sensor products; produced by the Japanese Ground Segment and delivered by EROS Data Centre in HDF format. The thermal infrared telescope operates in nadir-viewing, "whisk-

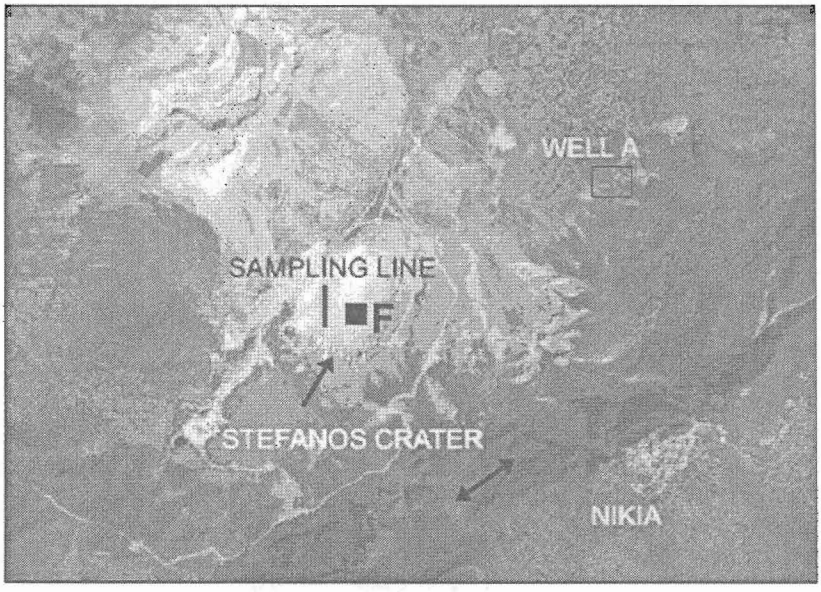

Figure 2. IKONOS-2 image of the Stefanos crater area (nadir view). The Stefanos Crater is the circular feature pointed at by the black arrow. The image has been orthorectified using a 2m DTM and GPS measurements (Vassilopoulou et al., 2002). The black features inside the crater show ground data sampling areas. Thin black box shows location of geothermal well A, drilled in 1982. Double-headed arrow points to NE-SW scarps on the eastern slope of the caldera. Letter F shows the fumarole region in the eastern part of the crater where degassing temperatures reach 100 degrees C.

broom" mode and collects emittance in five (5) channels having a 90 m spatial resolution. Figure 3 shows overviews of the ASTER scenes, daytime and night-time, respectively. The images show dark tones of grey over cool areas and bright tones over warm areas. There are notable differences between the two passes that in turn are associated with patterns of thermal structure, both ephemeral (sea) and permanent (land). A preliminary investigation of the thermal structure was made by observing emittance patterns in Figures 3 and 4. First, sunlit slopes (facing south, south-east) are warmer (brighter) on both images due to solar heating. This observation suggests an exposure effect (Kahle, 1987), which needs to be taken into account when retrieving surface temperatures. In addition, in the night image, there are sunlit slopes that show both warm and cold areas (see Figure 4 bottom). It is suggested that this is probably due to vegetation cover and rock type of those areas and needs further investigation, because it is related to emissivity variations. Secondly, the shape of the histograms is different: bimodal in the top image (day), unimodal in the bottom (night). This picture however may be coincidental due to the seasonal difference (April versus June). The top image has a wider range of radiance values (Table 2) than the bottom image. This is partly due to the fact that the left (cold) tail of the top histogram represents clouds. The mean value is higher in the bottom image, because the sea body is warmer. The sea is colder during daytime, but warmer than larger part of land areas during night-time.

2. Data Processing

2.1 ATCOR2 (Flat Surface Model)

The ASTER data were imported into GeomaticaT v8.2.1 as 16-bit unsigned integers.

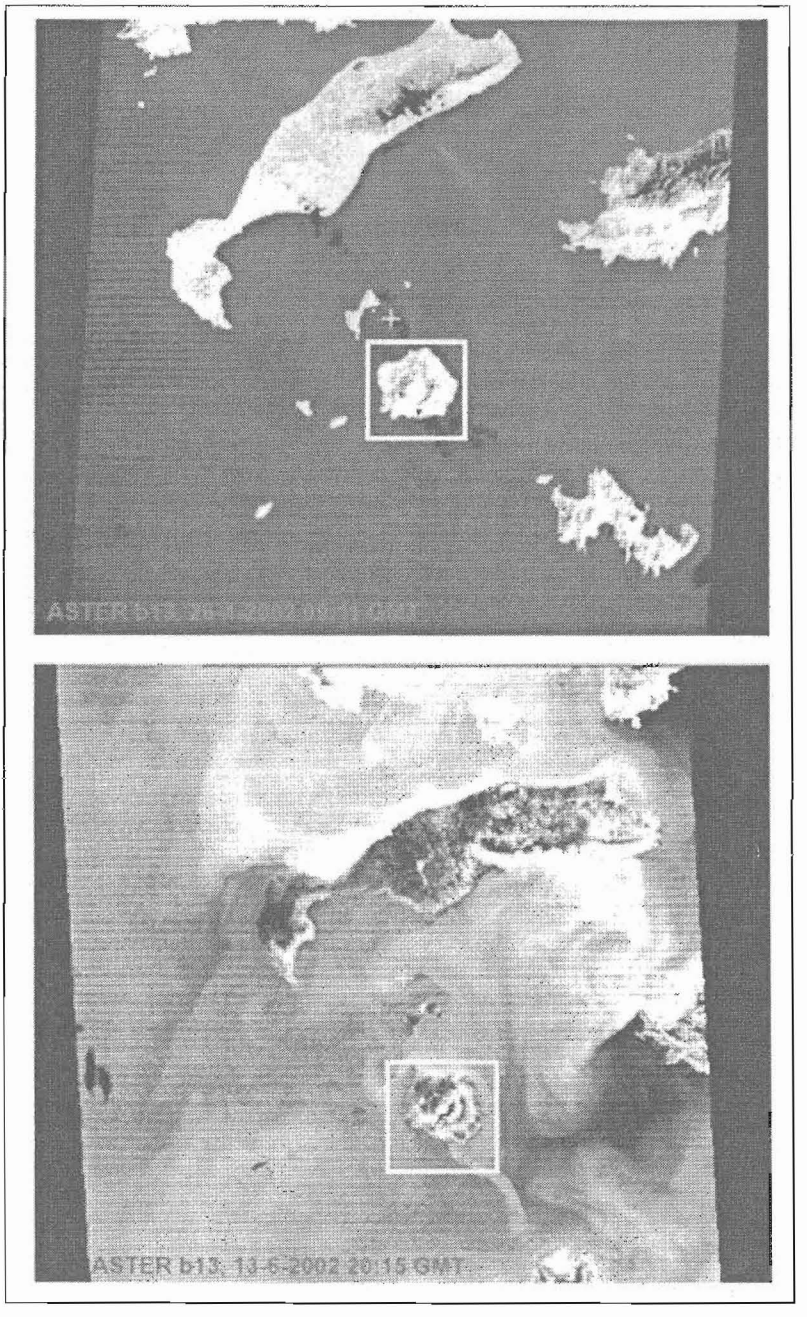

Figure 3. Monochrome overviews of the ASTER scenes of April 26 and June 13, 2002. Band 13 (thermal Infrared) is shown on both cases. Bright pixels indicate warm areas. Note the different orientation of the features due to the scanning mode of the sensor (descending-top, ascending-bottom). Box indicates extent of Figure 4.

Table 1. Detailed statistics of thermal images over Nisyros shown in Figure 4. Values reported are grey levels or

IMAGE	MEAN	SD	MIN	MAX
April 26, 2002 day*	1436.5	69.2	1155	1962
June 13, 2002 night	1500.30	9.2	1451	1584
Oct. 26, 2002 night	1534.75	30.9	1309	1562

*The extreme values for this day are due to the presence of clouds and their shadows.

All scenes were subsetted to smaller files (256 pixels x 256 lines or 128 x 128) thus including only Nisyros and surrounding sea. The files were exported to IMG format (16-bits), for ATCOR to be able to read them. No data scaling was done to 8-bit range, however, the computed temperature range is 8bit. The data were first processed using ATCOR2 (no 3-D correction) assuming a constant emissivity value of 0.98. A new calibration file was set up to establish the correct gain parameter **c1**. This was done using the band 13 conversion coefficient that can be found on the HDF metadata file:

$$\mathbf{c1} = \boldsymbol{incl}_{[x]} * 10^{-1}$$

where [x] = 0.005693 W/m² • sr • mm. This coefficient was the same for all images. We assumed a visibility of 15 km for all passes based on the meteorological data supplied to us by the Hellenic Meteorological Service (EMY). These data (Air Temperature, Dew Point, Relative Humidity, and Atmospheric Pressure) were collected at the Kos and Rhodes airports, every hour, at distances 25 and 80 km, respectively. Table 2 reports specific values at ground level for the time of each pass. TERRA passed over Nisyros at 09:11:55 GMT on April 26, 2002 (local time 12:11:55) and at 20:15:08 GMT on June 13, 2002 (local time 23:15:08). During October 2002 scene acquisition, a ground campaign took place with point temperature sampling from sites shown in figures 1 and 2. In addition, in situ meteorological data were collected from the local station established within the framework of the GEOWARN (www.geowarn.org) project inside Nisyros Caldera.

The ATCOR2 processing results are the following. The day scene (April 26, 2002; Fig. 4) was processed using the US standard-atmosphere model that matched better the meteorological ground data. The maximum value (44°C) was located on a sunlit slope of the volcano on the northeastern side, outside the caldera. The minimum values (3°C) were computed for the cloud pixels as expected. The sea surface temperature was 17 °C. The Stefanos crater surface temperatures were 32-33 °C, however, no thermal anomaly could

Table 2. Surface meteorological Data during TERRA passes over Nisyros. R is Rhodes Airport, K is Kos Airport.

DATE	TIME (Local)	TEMP (°C)	DEW POINT (°C)	HUM (%)	PRESSURE (hPa)	WIND SPEED (km/h)
April 26, 2002 R	12:20	19	9	52	1010	25.9
April 26, 2002 K	12:20	18	9	56	1010	25.9
June 13, 2002 R	22:20	24	19	73	1009	14.8
June 13, 2002 K	22:20	23	18	73	1010	11.1
Oct. 26, 2002 N	22:20	16	N/A	71	1015	N/A

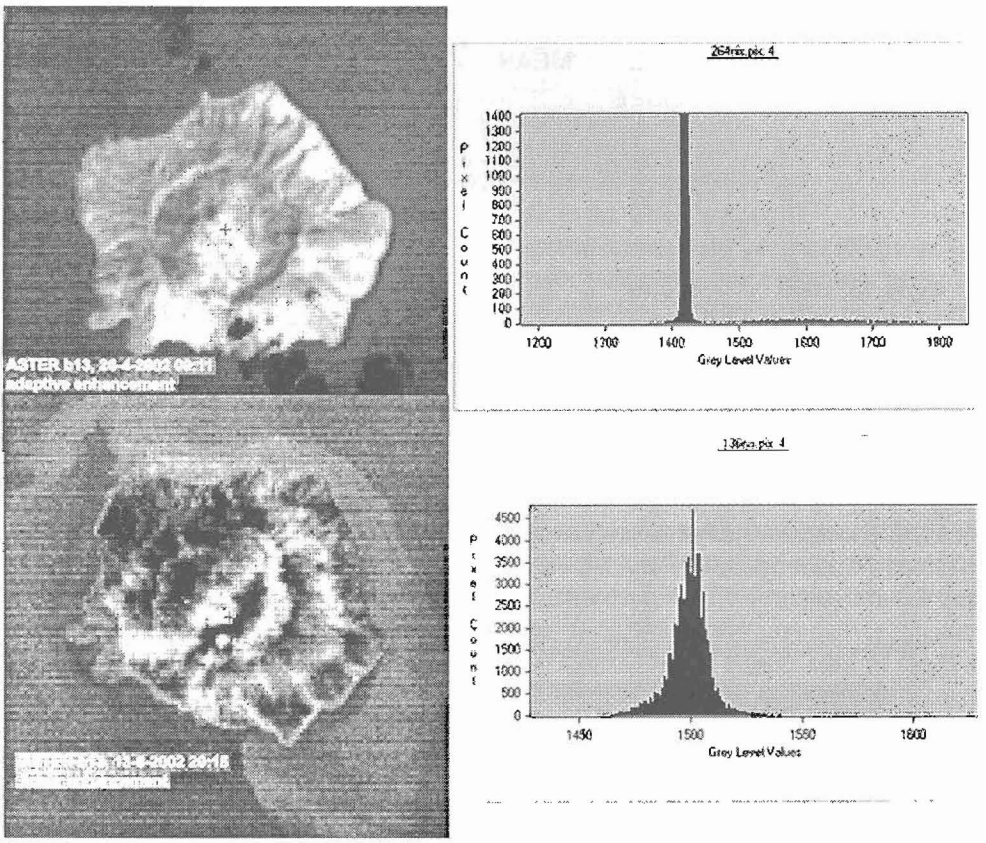

Figure 4. Monochrome overviews of the ASTER scenes of the Nissyros volcano of April 26 and June 13. Band 13 (thermal Infrared) is shown on both cases. Bright pixels indicate warm areas. Note the different orientation of the island due to the scanning mode of the sensor (descending-top, ascending-bottom). The histogram of pixel values (16-bit range) is also shown.

be detected because of solar heating. The first night scene (June 13, 2002; Fig. 4) was processed using the Mid-latitude summer atmospheric model. The maximum value (26 °C) was recorded inside Stefanos Crater. Minimum values (17 °C) were recorded on the northwestern flanks of the caldera. The sea-surface had temperatures ranging from 21-22 °C. The detailed temperature statistics of both images are shown in Table 4. Finally the temperature images were georeferenced to the UTM (zone 35) projection using a combination of two (2) reference vector files with RMS-X=0.38,0.53 and RMS-Y=0.57,0.39 pixels, respectively. First-order polynomials and Nearest Neighbor resampling were used.

The second night scene (October 26, 2002; Fig. 5) was processed using the Sub-arctic summer atmospheric model, which matched better our meteorological data on the ground. The maximum value (24 °C) over land was recorded inside Stefanos Crater. Minimum values (12 °C) were recorded on the western top of the caldera. It is noted that a similar range of values was also calculated on the October 2000 LANDSAT7 ETM+ scene of Nisyros (Ganas and Lagios, 2003) using a different atmospheric model. However, the 2002

Table 3. Detailed statistics of processed thermal im-

ATCOR2 Processed ASTER scene	PIXEL NUMBER	MEAN	SD	MIN	MAX
April 26, 2002 (Day)	65536	17.9	3.3	3	42
June 13, 2002 (Night)	65536	21.0	0.6	18	26
October 26, 2002 (Night)	22052	22.2	3.9	12	25

images show a temperature increase of 2 °C inside the Stefanos crater relative to previous work, which indicates thermal instability of this region over this two-year period. This is because the same processing software and emissivity value (0.98) on both epochs was used. On the other hand, the sea surface had temperatures ranging between 23 °C (near shore) 25 °C (open sea). Our ground

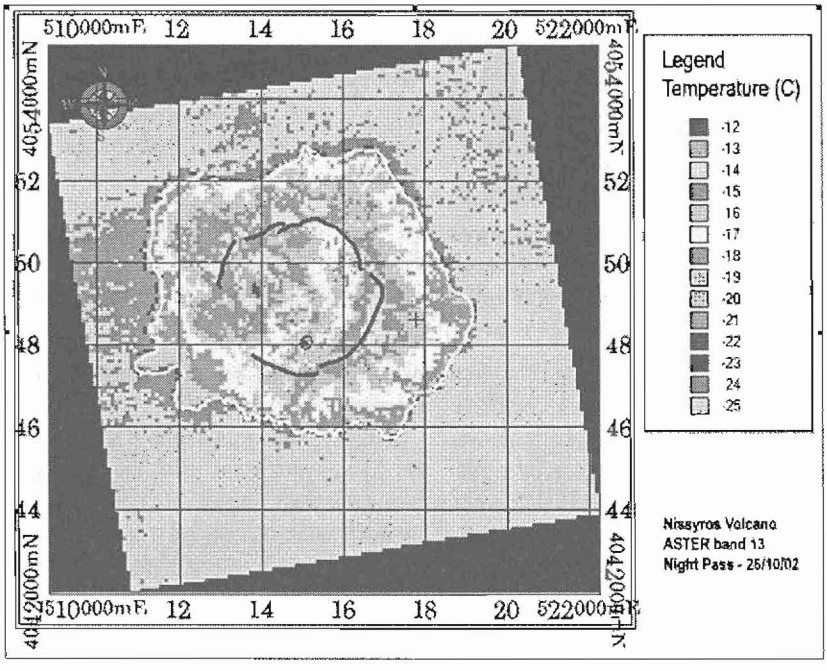

Figure 5. Colour overview of the processed ASTER scene of the Nissyros volcano acquired on 26 October 2002. A smooth colour pattern blue-green-red-purple corresponding to cold-medium-hot temperatures is shown. White line indicates the coastline and broken black line indicates the caldera rim. The Stefanos crater rim is indicated by the small black circle in the south of the caldera. Note the thermal anomaly (22-23 degrees C) inside the crater. Grid is UTM35.

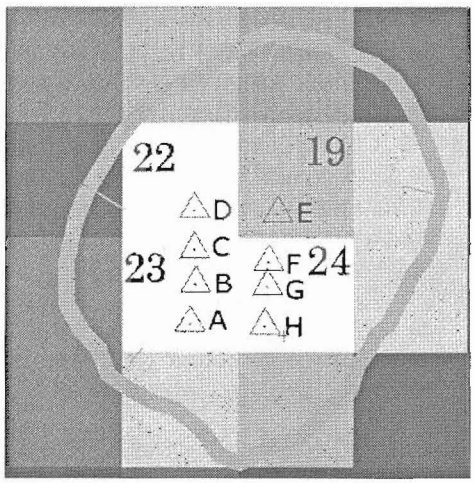

Figure 6. Temperature map of the Stefanos crater region calculated from the 26-10-2002 night scene after ATCOR2 processing. Increasing brightness indicates warmer surface temperatures. Green line with ticks shows the crater rim. Triangles indicate point sampling localities (A to H). Numbers represent average pixel temperature. Pixel size is 90 m.

measurements at points FARO and Palloi (Fig. 1) range between 23.1 °C and 23.4 °C. This comparison validates our results over those areas.

Although the thermal anomaly inside the crater was located, the extracted land surface temperatures showed mixed results when compared to actual ground data (Fig. 6). Our ground measurements were: point A 29.7 °C, point B 30.4 °C, point C 22.6 °C, point D 23.3 °C, point E 17.0 °C, point F 21.9 °C, point G 24.4 °C, and point H 33.5 °C. In other words, good matching exists for pixels 22, 19 and 24 (Fig. 6), while not satisfactory matching exists for pixel 23. The absolute deviation is 1.3 °C for pixel 22, 2 °C for pixel 19, 0.4-2.1 °C for points F and G against pixel 24, and 0.4-6.6 °C for pixel 23. The deviation regarding pixels 22, 19 and 24 may be due to the spatially averaging effect of the coarse ASTER pixel (90 m). The deviation for point H (pixel 24) and points A and B (pixel 23) is probably due to a subsurface effect that may increase surface temperature locally.

In general, it seems that the bottom half of the crater is warmer than the top half, in agreement with the October 2000 LANDSAT7 results of Ganas and Lagios (2003). This feature seems now permanent and is most likely due to the existence of an E-W fracture that crosses the crater. The fracture operates as a conduit for the ascent of fumarolic gases, which heats up the crater's surface. Near the Stefanos Crater, two shallow (up to 300 m depths) transitional conductivity zones having an E-W orientation, which may correspond to fracture zones, were deduced by Magneto-telluric soundings (Lagios, 1991)

The second factor affecting temperature accuracy is the spectral emissivity of the crater's surface. Because a unique value for the whole scene (0.98) was applied, the emissivity for the bare, volcanic surface of the crater, which is composed of mostly clay and pyroclastic layers, may be overestimated. ATCOR suggests this unique value probably underestimates surface temperatures by about 1.5 °C, although higher values (3-4 °C) are not unlikely. This constraint would increase extracted surface temperatures in figure 6 by at least 1.5 °C, which therefore would further reduce the temperature deviations discussed above.

3. Discussion-Conclusions

ASTER band 13 (10.25-10.95 mm; 90 m spatial resolution) was processed using scene-specific standard atmospheres from the ATCOR atmospheric Libraries. The results show a good comparison with previously processed LANDSAT7 ETM+ thermal data (Ganas & Lagios, 2003). The area of the main fumarolic activity on the island (Stefanos Crater; Chiodini et al., 2002) was clearly located (Fig. 5) and it was mapped warmer than the surroundings within the range of temperatures (22-24 °C) measured over previous campaigns. Despite the lack of ground data, it is suggested that the land surface temperature is probably underestimated inside Stefanos Crater (Fig. 2), because of the constant emissivity assumption. However, because of the overall agreement of these results with previous campaigns in Nisyros (Ganas

& Lagios, 2003), including the mapping of the "orographic effect" (Fig. 5), it is proposed that ASTER data may be successfully used to monitor the thermal status of the volcano.

In addition, the comparison of the ASTER thermal map for October 2002 to the LANDSAT7 thermal map for October 2000 (Ganas & Lagios, 2003) show that surface temperatures inside Stefanos Crater (Fig. 2) have risen on average by 2 °C within the period 2000-2002. This observation has to be also evaluated with respect to the increases in H_2 and CO contents of the fumaroles (Chiodini et al., 2002) indicated by geochemistry data between 1997-2001. The combination of increasing trends between geochemical and thermal data may indicate the onset of a new, unstable phase of the Nissyros volcano.

Acknowledgements

The EROS Data Centre (USA) and ERSDAC (Japan) provided the ASTER L1B data. This research was funded by GEOWARN (IST 12310-1999) project. We thank Dr. L. Maldonaldo, Mr. K. Haritos, Dr. G. Vougioukalakis, Dr. K. Nikolakopoulos, Mr. I. Bakopoulos, Dr. G. Stavrakakis, Prof. L. Hurni and Prof. V. Dietrich for their support and assistance. We also thank the project partners for many stimulating discussions.

References

Abrams, M., Hook, S., and Ramachandran, B., 2001. ASTER User Handbook, version 2. 135 pages.

Brombach, T., Hunziker, J. C., Chiodini, G., Cardellini, C., and Marini, L., 2001. Soil diffuse degassing and thermal energy fluxes from the southern Lakki plain, Nisyros (Greece). *Geophysical Research Letters*, **28**, 69-72.

Chiodini, G., Brombach, T., Caliro, S., Cardellini, C., Marini, L., and Dietrich, V., 2002. Geochemical indicators of possible ongoing volcanic unrest at Nisyros Island (Greece). *Geophysical Research Letters*, **29**, no. 16, 10.1029/2001gl014355, 2002

Ganas, A., & Lagios, E., 2003. LANDSAT7 thermal imaging of the Nisyros Volcano. *International Journal of Remote Sensing*, **24** (7), 1579-1586.

Geosystems Gmbh. ATCOR for ERDAS ImagineT User Manual, version 03/03/2002, 196 pages.

Harris, A. J. L., and Stevenson, D. S., 1997. Thermal observations of degassing open conduits and fumaroles at Stromboli and Vulcano using remotely sensed data. *Journal of Volcanology and Geothermal Research*, **76**, 175-198.

Kahle, A. B., 1987. Surface emittance, temperature and thermal inertia derived from Thermal Infrared Multispectral Scanner (TIMS) data for Death Valley, California. *Geophysics*, **52** (7), 858-874.

Lagios, E., 1991. Magnetotelluric Study of Nissyros Geothermal Field. *Bulletin of the Geological Society of Greece*, **25**, 393-407.

Lagios, E., 2000. Intense crustal deformation rates in Nisyros Island (Greece), deduced from DGPS studies, may foreshadow a forthcoming volcanic event. In: Balassanian, S., Cisternas, A., Melkumyan, M. (Eds.). *Proc. 2nd Int. Conf. On Earthquake Hazard & Seismic Risk Reduction.* Kluwer, Dordrecht, pp. 249-259.

Lagios, E., Dietrich, V., Stavrakakis, G., Parcharides, I., Sakkas V. & Vassilopoulou S., 2001. Will Nisyros Volcano (GR) become active? Seismic unrest and crustal deformation. *European Geologist*, **12**, 44-50.

Marini, L., Principe, C., Chiodini, G., Cioni, R., Fytikas, M., and Marinelli, G., 1993. Hydrothermal eruptions of Nisyros (Dodecanese, Greece). Past events and present hazard. *Journal of Volcanological and Geothermal Research*, **56**, 71 – 95.

Papadopoulos, G. A., Sachpazi, M., Panopoulou, G. and Stavrakakis, G., 1998. The volcanoseismic crisis of 1996 – 97 in Nisyros, SE Aegean Sea, Greece, *Terra Nova*, **10**, 151–154.

Papanikolaou, D., and Nomikou, P., 2001. Tectonic structure and volcanic centres at the eastern edge of the Aegean volcanic arc around Nissyros Island. *Bulletin of the Geological Society of Greece*, **34**, 289-296.

Richter, R., 1996. A spatially adaptive fast atmospheric correction algorithm. *International*

Journal of Remote Sensing, **17** (6), 1201-1214.

Sachpazi M., Kontoes, Ch., Voulgaris, N., Laigle, M., Vougioukalakis, G., Sikioti, O., Stavrakakis, G., Baskoutas J., Kalogeras, J., and Lepine, J. Cl. 2002. Seismological and INSAR signature of unrest at Nisyros Caldera, Greece. *Journal of Volcanological and Geothermal Research*, **116**, 19-33.

Thome, K., Palluconi, F., Takashima, T., and Masuda, K., 1998. Atmospheric correction of ASTER. *IEEE Transactions on Geoscience and Remote Sensing*, **36** (4), 1199-1211.

Vassilopoulou, S., Hurni, L., Dietrich, V., Baltsavias, M., Pateraki, M., Lagios, E., Parcharidis, Is. 2002. Ortho-Photo Generation using IKONOS-2 Imagery and High Resolution DEM: A case study on monitoring the Volcanic Hazard on Nissyros Island (Greece). *ISPRS Journal of Photogrammetry and Remote Sensing*, **57**, 24-38.